Electrochemical properties of the interaction between cytochrome *c* and a hematite nanowire array electrode

Hanyu Wang[1], Alexander Johs[2], James F. Browning[1], David Alan Tennant[3], Liyuan Liang[2,*]

[1] Neutron Scattering Division, Oak Ridge National Laboratory, P.O. Box 2008, Oak Ridge, TN 37831, U.S.A.

[2] Environmental Sciences Division, Oak Ridge National Laboratory, P.O. Box 2008, Oak Ridge, TN 37831, U.S.A.

[3] Materials Science and Technology Division, Oak Ridge National Laboratory, P.O. Box 2008, Oak Ridge, TN 37831, U.S.A.

Abstract

We investigate the interaction of horse heart cytochrome *c* (cyt *c*) with hematite nanowire array electrodes by cyclic voltammetry to study the electron transfer between redox active proteins and mineral surfaces. Using this model system, we quantify electron transfer rates between cyt *c* and hematite under varying electric potential and pH conditions. The results are consistent with two distinct cyt *c* conformations adsorbed at the hematite surface: the native and a partially unfolded form. The partially unfolded protein maintained redox activity, but at a lower redox potential than the native protein. Adsorption of cyt *c* allowed direct electron transfer between cyt *c* and hematite, with an interfacial electron transfer rate, k^o_{ET}, of 0.4 s^{-1} for the native form and 0.55 s^{-1} for the partially unfolded protein at pH 7.07. In pH 4.66 solutions, cyt *c* adsorption decreased compared with the neutral solution and the fraction of partially unfolded protein increased. Additionally, the diffusion controlled electron transfer rate between hematite and the electron shuttling compound anthraquinone-2,6-disulfonate (AQDS) was determined to be $k^o_{ET} = 8.0 \cdot 10^{-3}$ $cm \cdot s^{-1}$ at pH 7.07. Modulation of electron transfer rates as a result of conformational changes of redox active proteins has broad implications for describing molecular scale chemical transformations at biological-mineral interfaces.

Keywords: Hematite; Cytochrome; Electron transfer; Cyclic Voltammetry; Adsorption

1. Introduction

The demand for energy-efficient processes for wastewater treatment can be met by simultaneously recovering the chemical energy in wastewater by microbial fuel cells (MFC) [1]. Yet, their relatively low output voltage and power density compared to other energy conversion devices limit the practical application of MFCs as power generators. In order to overcome the thermodynamic constraints without increasing operational cost, researchers have attempted to couple solar energy devices with MFC technologies to enable efficient utilization of multiple energy sources [2, 3]. A single solar-MFC device that employs a photoanode interfaced with a microbial biofilm has been reported to enable efficient electrical conduction between the photoanode-cell interface [4]. The greatly increased photocurrent generation was evidently

affected by interaction between a hematite electrode and electrogenic bacterial strains among *Shewanella* species. These results highlight the central importance of the microbe-mineral interface. However, knowledge regarding molecular-level processes at the complex biological-semiconductor interface remains limited. It is essential to unravel the mechanisms governing direct electron transfer between proteins and minerals, particularly the influence of chemical gradients, protein sorption and the role of protein conformation at interfaces. Such insights will advance molecular-level understanding of the complex microbial-semiconductor interface.

Extracellular electron transfer by dissimilatory metal-reducing bacteria (DMRB), such as *Geobacter sulfurreducens* PCA and *Shewanella oneidensis* MR-1, involves a series of multiheme cytochromes [5-7]. These mostly membrane-associated redox proteins shuttle electrons from the inner membrane across the periplasmatic space and through the outer membrane to a terminal electron acceptor [e.g. Fe(III)] [8]. One of several possible pathways by which dissimilatory iron-reducing bacteria transfer electrons to solid mineral electron acceptors is through direct contact between redox-active cytochromes and mineral surfaces [9]. The *c*-type cytochromes involved in interactions with mineral surfaces and electron transfer processes are of particular interest, including outer membrane cytochromes of DMRB, such as OmcA and MtrC [10, 11], as well as mitochondrial cytochrome *c* (cyt *c*) [12, 13]. A key difference between bacterial outer membrane cytochromes and mitochondrial cyt *c* is the number of hemes and the coordination of Fe in the heme moieties. Outer membrane cytochromes contain 10-11 hemes with axial *bis*-histidine-coordinated Fe, whereas cyt *c* contains only a single heme with axial histidine-methionine Fe coordination (Figure 1) [6]. Cyt *c* has been a focus of research for many years, as it is functionally involved in the electron transport chain of mitochondria and plays essential roles in key cellular processes, such as apoptosis [14]. Furthermore, cyt *c* can be used as a model system to study the interactions of redox-active proteins with minerals and electron transfer processes between heme moieties and external electron acceptors, analogous to the interaction of outer membrane proteins from DMRB with minerals [15, 16].

The interfacial electrochemistry of horse heart cyt *c* at different types of electrodes, including metal electrodes and metal oxide electrodes, has been investigated previously [17]. The results show that cyt *c* is capable of transferring electrons rapidly with unmodified gold, platinum, tin oxide, and indium oxide electrodes. The reaction rates were strongly dependent on solution conditions, electrode pretreatment procedures, experimental protocol, and the surface conditions of the electrodes. Self-assembled monolayers (SAMs) prepared with COOH-terminated alkanethiols ($HS(CH_2)_n$-COOH) can serve as excellent modifiers of gold surfaces for the immobilization of cyt *c* in a stable electroactive state [18]. However, for SAMs assembled using alkanethiols with an alkyl chain length $n \geq 8$, the standard electron-transfer rate decreases exponentially with n. When $n = 15$, the rate constant at zero overpotential is 0.1 s^{-1}, and this value is 10-100 times smaller than that for the cyt *c* and tin oxide system.

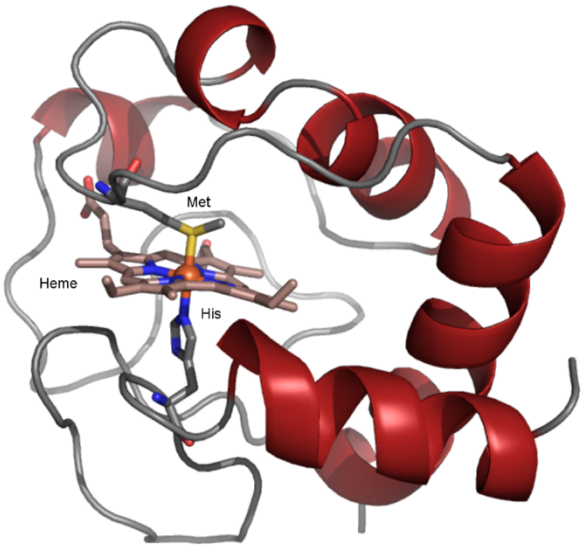

Figure 1: Molecular structure of mitochondrial horse heart cytochrome *c*. The heme moiety and methionine (Met) and histidine (His) residues coordinated to the Fe center are shown in a stick representation (Protein Data Bank identification code: 1HRC).

The spatial arrangement of proteins on electrodes has also been widely studied to take advantage of three-dimensional (3D) conduction pathways, as well as scaffolds for protein immobilization. 3D gold nanoparticle-modified electrodes have been fabricated to obtain densely immobilized cyt *c* on its surface with direct, reversible electron transfer [19]. Previous studies found that electron transfer to mineral surfaces is controlled by the mode of interaction between cyt *c* with electron acceptors or donors. Experimental evidence suggests that cyt *c* can adopt various conformations upon interaction with binding partners and adsorption to surfaces [16]. Electrochemical data indicate that cyt *c* undergoes a conformational change upon adsorption to indium-tin oxide electrodes [12]. This adsorption-induced conformational change was corroborated in another study with hematite and indium-tin oxide electrodes [20]. Although interactions between *c*-type cytochromes and hematite surfaces have been characterized [15, 20], the electron transfer rate of cyt *c* at the hematite electrode surface has not been determined.

Self-secreted and exogenous electron accepting/donating compounds, such as quinones, represent an alternative mechanism of extracellular electron transfer, which can support and complement direct electron transfer processes and significantly increase effective electron transfer rates [21]. Small molecule electron shuttles include riboflavin (RF), flavin mononucleotide (FMN), and anthraquinone-2,6-disulfonate (AQDS). Laboratory studies have demonstrated the role of flavins as electron shuttle compounds, enhancing the ability of *S. oneidensis* to respire insoluble substrates [22]. RF and FMN were shown to increase electron transfer by interacting with specific binding sites in outer membrane *c*-type cytochromes [23, 24]. Among the electron shuttling compounds, AQDS was shown to be a particularly effective mediator due to its low half-cell potential and fast redox kinetics in both forward and reverse directions [25]. The proposed mechanism for electron transfer enhancement by AQDS involves

reduction of oxidized AQDS by dissimilatory iron-reducing bacteria (DIRB) with H_2 as electron donor. Subsequently, the reduced form AH_2DS shuttles electrons to Fe(III) oxide, where it is oxidized back to AQDS through heterogeneous surface electron transfer. The addition of AQDS to DIRB cells stimulated Fe(III) reduction by removing the need for microbes to directly contact minerals [26, 27]. While AQDS is known to enhance the reduction of Fe(III) oxides in whole cell studies with DIRB, its redox kinetics at the Fe(III) oxide interface is not well characterized.

In this study, we selected horse heart cyt *c* as a model protein to study the direct electrochemistry at the protein-mineral interface. The structure and heme moiety of cyt *c* are well defined and the protein can be studied within a wide range of conditions, such as solution pH, protein concentrations and applied potentials. The structure and folding states of cyt *c* have been linked to electrochemical characteristics that allow us to correlate electrochemical observations with the conformational states of the protein while adsorbed to a solid surface. Hematite, an abundant, poorly soluble, and stable form of iron oxide, is investigated in this study due to its significant role in biogeochemical redox processes such as dissimilatory metal reduction by iron-reducing bacteria [28-30], and its favorable band gap for solar light absorption, chemical stability and, more importantly, biocompatibility with cytochromes [4, 31]. We present electrochemical evidence that cyt *c* assumes at least two conformations upon interaction with hematite. We evaluated sorption characteristics of cyt *c* as a function of concentration and pH, and determined the rate constants of electron transfer at the interface of cyt *c* and hematite. Additionally, we studied the electron transfer of the small redox mediator AQDS with the hematite electrode to evaluate hematite as a semiconductor electrode material. The intrinsic band gap of hematite limits conductivity making it a challenging electrode material. Determining electron transfer rates between AQDS and hematite electrodes in relation to more common electrode materials enables us to assess the impact of the natural mineral characteristics on electron transfer rates. AQDS is widely used as a redox mediator in studies to investigate electron shuttling between microbes and iron oxides.

2. Materials and methods

All experiments, except the hydrothermal synthesis of iron oxyhydroxide (goethite, β-FeOOH) nanowires, were conducted in a glovebox under a high-purity nitrogen atmosphere (<1 ppm O_2). All glassware for wet chemical experiments was rinsed with milli-Q water (~18 MΩ·cm) several times before use. To remove oxygen in the water, milli-Q water was boiled and purged with nitrogen gas for 30 min while stirring with a stir bar. It was then transferred to an ice bath with continued stirring and purging. Deoxygenated milli-Q water was stored in the glovebox and filtered through a 0.22 μm sterile filter for the preparation of all solutions. Cytochrome *c* from equine heart (≥95%) purchased from Sigma-Aldrich Co. was used without further purification. All other chemicals used were reagent grade. All chemicals, plastic syringes, syringe filters, glass tubes, vials and pipette tips were deoxygenated inside the glovebox for at least 24 hrs before use.

2.1 Synthesis of hematite nanowire-arrays

Dense and vertically aligned hematite nanowire arrays were grown on a fluorine-doped tin oxide (FTO)-coated glass substrate, using a hydrothermal method as previously reported, with slight modification [4]. Briefly, 20 ml aqueous solution containing 0.15 M of ferric chloride and 1 M sodium nitrate at pH 1 (adjusted by HCl) was added into a 30-mL stainless steel autoclave with a Teflon liner. A cleaned FTO glass substrate was placed in the solution of the autoclave, and then heated at 95 °C for 4 hrs. The autoclave was cooled to room temperature. The substrate was covered with a uniform layer of goethite (β-FeOOH) nanowire film (yellow color). The β-FeOOH coated substrate was washed with deionized water, and then air dried. To obtain crystalline hematite (α-Fe_2O_3), the β-FeOOH nanowire arrays were calcined at 550 °C for 2 hrs in a horizontal quartz-tube furnace, which was filled with ultrahigh purity N_2 (99.998%, Praxair) at a pressure of 740 Torr. The β-FeOOH nanowires were converted into α-Fe_2O_3 nanowires, and the color of the film changed from yellow to red. The morphology and identity of the synthesized mineral on the FTO substrate were characterized by SEM imagining and XRD pattern (Figure S1). The hematite nanowires have an average diameter of 30 nm and an average length of 1000 nm.

2.2 Electrochemical Measurements

A three-electrode system was constructed to carry out the electrochemical measurements, using a working electrode consisting of hematite nanowires on an FTO-coated glass substrate, Ag/AgCl (sat. KCl) as the reference electrode, and a platinum wire as the counter electrode. All reported potentials are relative to the Ag/AgCl reference potential. A deoxygenated buffer containing 20 mM Tris-HCl (pH 7, unless stated otherwise) was used, with 150 mM NaCl as the electrolyte. The electrodes were immersed in the buffer solution containing cyt *c* for about 30 min before each measurement, to allow the cytochromes to reach sorption equilibrium with the hematite surface. Cyclic voltammograms (CV) were taken at a scan rate of 10 $mV \cdot s^{-1}$ (unless otherwise specified) using a BioLogic SP-300 electrochemical potentiostat (BioLogic Science Instruments, Grenoble, France). All hematite electrodes were fabricated by attaching a copper wire to the bare edge of the FTO glass substrate by soldering a small piece of indium metal, followed by sealing the FTO glass substrate and metal contact region with insulating epoxy resin. The surface area of the hematite nanowire array working electrode was projected to be 5–10 cm^2. All electrochemical measurements were carried out at room temperature in a glovebox under a N_2 atmosphere (< 1 ppm O_2). The experiments were run in triplicate and with blank and control experiments.

2.3 Analysis of CV data

The amount of cyt *c* (mol) adsorbed on the hematite electrode was calculated by using the total charge derived from the redox peaks in the cyclic voltammograms, on the basis that cyt *c* has one heme. The charge was calculated by integrating the area under the cathodic curve after subtracting the cathodic curve of the control, which was the CV trace of the hematite electrode in the absence of cyt *c*. The molarity of the cyt *c* sorption on hematite was then calculated based on the projected surface area of the hematite electrode.

To derive the electron transfer rates, multiple CV traces were taken at increasing scan rates. With these CV measurements over a large range of scan rates, the results can be displayed by plotting E_{pa} (anodic peak potential) and E_{pc} (cathodic peak potential) as a function of scan rate (a 'trumpet plot'). Data in the trumpet plot were analyzed using the program Jellyfit [32]. Jellyfit offers

several electron-transfer models to fit experimental data, including a Butler-Volmer description of a single adsorbed redox center, based on the method described by Laviron [33], which was used to fit the trumpet plots over the entire range of scan rates to determine rate constants.

3. Results and Discussion

3.1 Interaction of AQDS with a hematite electrode

Cyclic voltammetry (CV) measurements were carried out under anoxic conditions to evaluate electron transfer at the electrode interface. We used a hematite nanowire array working electrode and focused on a potential window between -0.6 and 0.5 V versus Ag/AgCl, in which the hematite is electrochemically stable [4]. To evaluate the performance of the hematite electrode and to characterize the interaction of AQDS with hematite, we conducted CV measurements in Tris-HCl buffer solutions (pH 7.07) containing 20 μM AQDS (red line, Figure 2a). The CV trace of the hematite electrode in Tris-HCl buffer as a background control is also shown in Figure 2a (black dashed line). Compared to the control, the CV trace of AQDS shows a cathodic peak potential (E_{pc}) of -464 mV and an anodic peak potential (E_{pa}) of -398 mV against Ag/AgCl (Figure 2b). The midpoint potential ($E^{0'}$) of -431 mV can be calculated according to $E^{0'} = (E_{pc} + E_{pa}) / 2$.

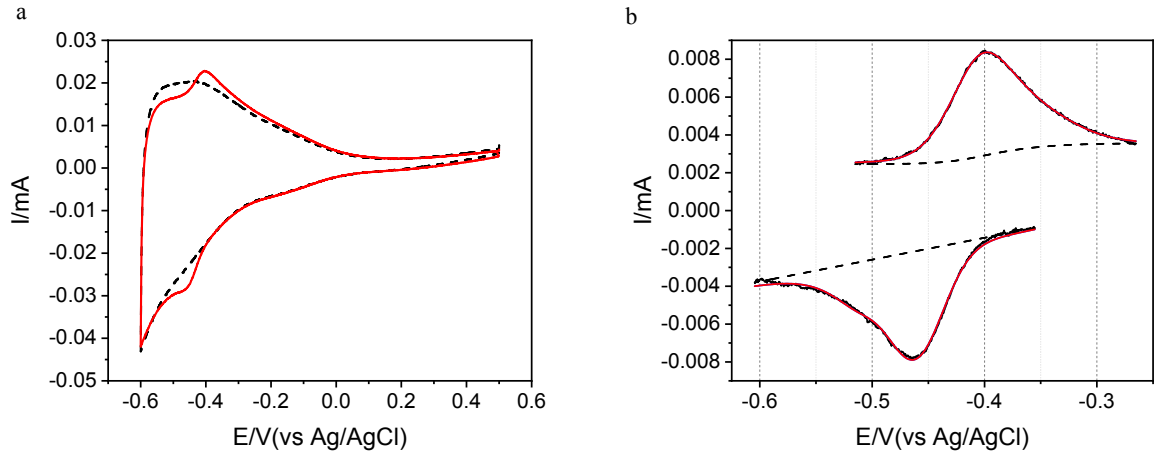

Figure 2. (a) Cyclic voltammetry data collected from a hematite nanowire electrode, using a background solution of Tris-HCl buffer at pH 7.07 (black dashed line) and 20 μM AQDS in Tris-HCl buffer (red solid line). The scan rate is 10 $mV \cdot s^{-1}$ and Ag/AgCl (sat. KCl) is the reference electrode. (b) The same reduction curves from CV data in (a) after background subtraction and peak deconvolution. Each line represents: raw peak (black), background (dashed black), AQDS (red). A pair of redox peaks of AQDS is obtained: cathodic peak at -464 mV, and anodic peak at -398 mV.

The pronounced pair of redox peaks can be attributed to AQDS resulting from electron transfer between AQDS and the hematite nanowire array electrode [34, 35]. The difference between the reduction and oxidation peak potentials is close to 60 mV, which signifies the existence of a fully electrochemically reversible redox couple, implying that the semiquinone redox state (AQDSH,

$AQDS^-$) is present in the redox system [36]. Furthermore, we expect that the diffusion-controlled reaction occurs at the aqueous interface of the hematite electrode because sorption of AQDS to hematite is negligible at neutral pH (See Figure S2) [25]. Through use of the Randles-Sevcik equation which describes the effect of scan rate on the peak current i_p [37], the diffusion coefficient for AQDS was estimated as $6.15 \cdot 10^{-5}$ $cm^2 \cdot s^{-1}$. The observed Nernstian behavior of AQDS and its reduction potentials indicate that the hematite working electrode performs as expected. Furthermore, the nanowire array electrode used in this study is much more robust than monolithic hematite electrodes used previously [20], as we observed smaller variability (within 15 mV) in the redox peaks between experiments.

3.2 Interaction between cyt *c* and hematite by CV measurements

To investigate the electrochemical interaction of cyt *c* with hematite, we conducted CV measurements of cyt *c* in Tris-HCl buffer solutions using the hematite nanowire array electrode. In Figure 3a, the CV trace of the hematite electrode is compared with that of cyt *c,* both in Tris-HCl buffer (pH 7.07). Compared with the buffer control, cyt *c* shows obvious redox peaks in the potential range between -400 mV and 200 mV. After linear background subtraction and deconvolution of the CV curves, two pairs of redox peaks can be identified (Figure 3b). An anodic peak (E_{pa}) at 120 mV and a cathodic peak (E_{pc}) at -150 mV were attributed to the native form of cyt *c* (magenta line). The other pair, with an E_{pa} at -195 mV and an E_{pc} at -360 mV, can be attributed to the partially unfolded form of cyt *c* (blue line) [20]. The midpoint potential values at the neutral pH ($E^{0'}$) are -15 mV and -278 mV for the native and the partially unfolded form of cyt *c*, respectively. These redox peaks represent the electron transfer between the cytochrome and hematite; and the values are similar to the reported potentials of -120 mV and -400 mV (cathodic scan for native and partially unfolded cyt *c*) using a natural hematite electrode in a neutral medium [20].

a

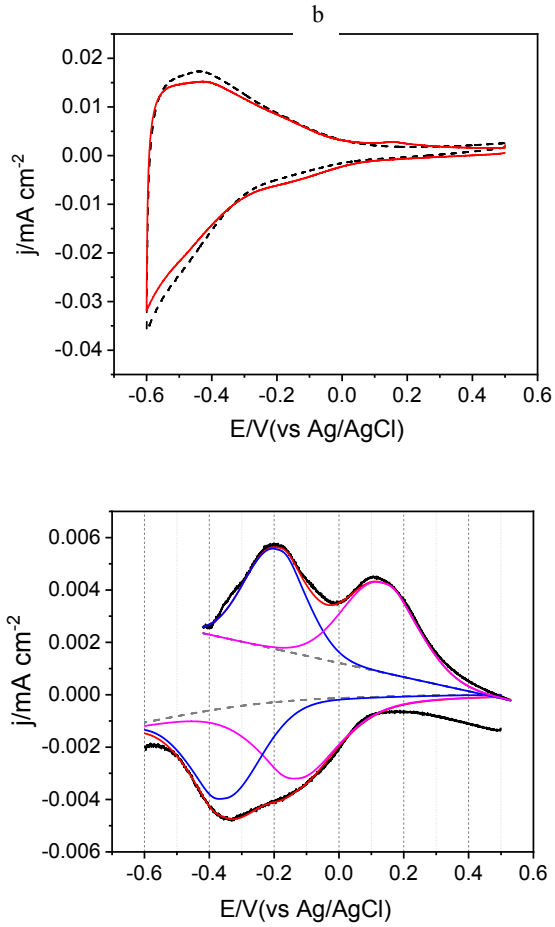

Figure 3. (a) Cyclic voltammetry data collected from a hematite nanowire array electrode, using a background solution of Tris-HCl at pH 7.07 (black dashed line) and 40 µM cyt *c* in Tris-HCl buffer (red solid line). The scan rate is 10 $mV \cdot s^{-1}$ and Ag/AgCl (sat. KCl) is the reference electrode. (b) The same reduction curves from the CV data in (a) after background subtraction and peak deconvolution. Each line represents: raw data (black), background (dashed black), peak sum (red), native form of cyt *c* (magenta) and partially unfolded form of cyt *c* (blue). Two pairs of redox peaks are obtained, which are attributed to the native form (E_{pc} = -150 mV and E_{pa} = 120 mV), and the partially unfolded form (E_{pc} = -360 mV and E_{pa} = -195 mV) of cyt *c*.

Unlike the diffusion-controlled reaction at the hematite electrode interface for the small redox molecule AQDS, cyt *c* readily adsorbs on hematite surfaces and interacts with hematite electrodes as the adsorbed protein species (Khare et al., 2006). Indeed, the reduction and oxidation peaks are separated by more than 60 mV. Thus, on hematite surfaces, cyt *c* redox processes are not completely electrochemically reversible (Chen et al., 2002; Khare et al., 2006). Using SAMs with methyl-terminated alkanes on gold electrodes Chen et al. [38] also reported changes in the orientation and conformation of the cyt *c* proteins adsorbed on the electrode. The authors observed a large shift in the reduction potential to -320 mV and suggested that cyt *c* was denatured upon adsorption on the SAM surface. Since this low potential is close to that of aqua-heme, which is the form obtained after displacing the methionine axially coordinated to the heme

Fe with a water molecule, [20, 39], it has been interpreted as unfolding of the protein, exposing the heme group [15].

In our case, sorption did not cause cyt *c* to lose redox activity, or an irreversible shift in the redox potential that has been observed for fully denatured cyt *c* [38]. Instead, interaction between cyt *c* and the mineral surface triggered a conformational change, rather than yielding fully denatured protein that results in altered redox properties [40]. Therefore, we attribute the lower potential shift to a partially unfolded conformation of cyt *c*, which was caused by its adsorption on the hematite electrodes. The resulting protein conformation may partially expose its heme group likely by breaking the weak Fe-S coordination displacing the axially coordinated methionine with a water molecule or a hydroxyl ion. This new environment surrounding the heme group may account for the lower reduction potential than its native conformation, where the heme is screened by the protein scaffold. These results therefore suggest that cyt *c* interacts with hematite in two electrochemically distinct forms.

3.3 Effect of pH on cyt *c* and its interaction with hematite

The effect of buffer pH on the midpoint potential and conformation of cyt *c* was evaluated, as the molecular conformation of horse heart cyt *c* is dependent on solution conditions, especially pH [41]. Figure 4 shows the cyclic voltammetry data of cyt *c* on hematite nanowire array electrodes at pH 4.66 as compared to that at pH 7.07 shown in Figure 3. At near neutral pH, we observed a pair of redox peaks with midpoint potentials $E^{0'}$ of -15 mV and -278 mV for the native and the partially unfolded forms of cyt *c* as discussed above. In comparison, the cyclic voltammogram of cyt *c* appears to be relatively flat at acidic pH (Figure 4a). After linear background subtraction and deconvolution of the CV curves, we identified two pairs of redox peaks (Figure 4b): a cathodic peak at -130 mV and anodic peak at 60 mV, yielding $E^{0'}$ of -35 mV for native form of cyt *c*; and a cathodic peak at -350 mV and anodic peak at -205 mV, with $E^{0'}$ of -278 mV for the partially unfolded form of cyt *c*. It has been reported that the molten globule-like (partially unfolded) state of cyt *c* can be induced by moderately lowering the pH [42]. Therefore, we infer that lowering pH induces a cooperative conformational change in cyt *c*, consistent with previous reports [43].

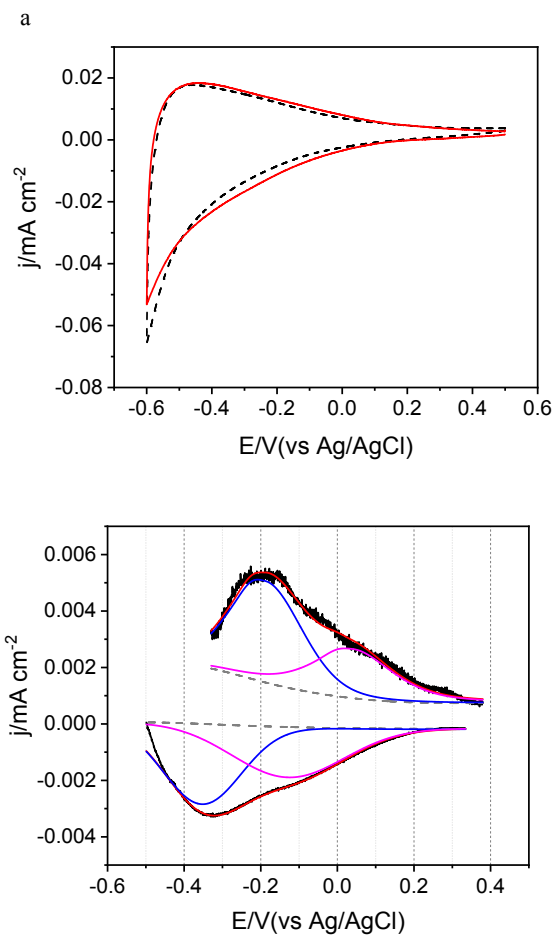

Figure 4. (a) Cyclic voltammetry data collected from a hematite nanowire array electrode, using a background solution of Tris-HCl at pH 4.66 (black dashed line) and 40 µM cyt *c* in Tris-HCl buffer (red solid line). The scan rate is 10 $mV \cdot s^{-1}$ and Ag/AgCl (sat. KCl) is the reference electrode. (b) The CV data from (a) after background subtraction and peak deconvolution. Each line represents raw data (black), background (dashed black), peak sum (red), native form of cyt *c* (magenta) and partially unfolded form of cyt *c* (blue). At pH 4.66, the two pairs of redox peaks are attributed to the native conformation (E_{pc} = -130 mV and E_{pa} = 60 mV), and the partially unfolded conformation (E_{pc} = -350 mV and E_{pa} = -205 mV) of cyt *c*.

The peak current of native cyt *c* at a modified gold surface showed a similar dependence on pH [44]. As the pH was lowered from 7.5 to 3, the peaks in the CV curve became broader with a concomitant decrease in peak current, reaching zero close to pH 4. The observed changes in the peak current within the investigated potential window suggest that cyt *c* immobilized on the hematite surface is more susceptible to unfolding at acidic pH. This unfolding, in particular, alters the heme binding pocket and its exposure to solvent [15, 40]. Apart from affecting the conformation of cyt *c*, pH also affects the surface properties of the hematite electrode. Similar to Shimizu et al. (2012), we observed a high cathodic current density, 0.07 $mA \cdot cm^{-2}$ as pH decreased to 4.66 (Figure 4a) compared to 0.035 $mA \cdot cm^{-2}$ at pH 7.07 (Figure 3a), which was

attributed to reductive dissolution of hematite [45]. The main effect of pH relevant to our study, however, is on the conformational change of cyt *c*. The resulting structural rearrangement can modulate the electrochemical properties and electron transfer kinetics, which is explored in section 3.5 below.

In addition, we performed CV measurements of cyt *c* at an alkaline pH of 9.8. The CV trace showed significantly decreased current density across the entire investigated potential window (Figure S3), compared to neutral or acidic conditions. A similar effect due to elevated pH was reported previously [46]. The data suggest that the reduced current density may be caused by partial oxidation of Fe(III) sites on the surface of hematite, resulting in the formation of an insulating Fe(IV) layer under alkaline conditions [45]. Due to the substantial reduction (60%) in current density caused by surface chemistry change of the hematite electrode, we focused on the electrochemistry of cyt *c* at neutral and acidic pH values.

3.4 Sorption of cyt *c* and its interaction with hematite

Sorption and surface density of cyt *c* are important factors to consider because they can affect the electron transfer between the protein and hematite surfaces. We investigated the influence of the solution pH on the amount of cyt *c* adsorbed on the surface of the hematite electrode. We carried out experiments to obtain CV data as a function of cyt *c* concentration. For each experiment, the electrodes were allowed to equilibrate with the cyt *c* solution for 30 min before taking the CV measurements. The maximal currents for cathodic waves increased as the concentration of cyt *c* increased from 20 μM to 880 μM in a potential range of -400 mV to 0 mV versus Ag/AgCl (see Supporting Information, Figures S4–S6). At the highest cyt *c* concentration of 880 μM the current plateaued in both neutral and acidic media, indicating that sorption of cyt *c* on the hematite electrode reached saturation. The amount of cyt *c* adsorbed on the hematite surface ($\mu mol \cdot m^{-2}$) was determined by integrating the area under the cathodic curve after subtracting the cathodic curve of the control, which was the CV trace of the hematite electrode in the absence of cyt *c*. The sorption isotherm of cyt *c* on the hematite nanowire-array electrode is shown in Figure 5. The monolayer adsorption capacity was extrapolated from the Langmuir fit to the experimental data.

$$Y = \frac{Q_m \cdot b \cdot C_{eq}}{1 + b \cdot C_{eq}} \quad (1)$$

Where Q_m ($\mu mol \cdot m^{-2}$) is the monolayer adsorption capacity, C_{eq} is the concentration of cyt *c* in solution with unit (μM), *b* is the Langmuir constant, and *Y* ($\mu mol \cdot m^{-2}$) is the amount of cyt *c* adsorbed on the sorbent surface.

From Figure 5, it can be clearly seen that adsorption of cyt *c* is affected by the pH of the solution. The sorption capacities of cyt *c* on the hematite were determined from Langmuir fits to the experimental data and amount to 23.38 $\mu mol \cdot m^{-2}$ at pH 7.07 and 8.17 $\mu mol \cdot m^{-2}$ at pH 4.3. Assuming cyt *c* arrangement in a single monolayer, the surface coverage corresponds to 14 and 5 protein molecules per nm^2 of surface area at pH 7.07 and pH 4.3, respectively, which are quite high values considering the molecular dimensions of the globular cytochrome of 30×34×34 $Å^3$ [47]. This is because the projected surface area of the electrode was used in the calculation, rather than the much larger textured surface area of the hematite nanowires. Accounting for the average length (1000 nm) and width (30 nm) of individual hematite nanowires covering the 1-

cm^2 substrate surface, the accessible surface area of the electrode can reach a value of up to 135 cm^2. Using this more realistic estimate of the hematite nanowire surface area, we obtained a corrected surface coverage of 0.103 molecules/nm^2 and 0.037 molecules/nm^2, respectively, for pH 7.07 and 4.3. Considering that one cyt *c* occupies an average surface area of 9.07 nm^2, we calculated the monolayer coverages of cyt *c* on effective surface area of hematite nanowires to be about 93% at pH 7.07 and 33% at pH 4.3, respectively.

The isoelectric point (pI) of horse heart cyt *c* is 10.2, whereas the pH of zero-point charge, pH_{zpc}, of hematite is ~8.5 [48]. Between pH 7-10, the protein is positively charged and the charge of the mineral surface transitions from weakly positive, to neutral, and then negative. Thus, sorption at pH 4 and 7 is mostly unfavorable due to electrostatic repulsion, which is as a result of an excess of positively charged lysine and arginine residues resulting in a net positive charge of +8 for horse heart cytochrome *c*. However, the electrostatic interactions of the protein are determined by the spatial distribution of basic and acidic amino acid residues, some of which may be screened by oppositely charged ions in our system. As the protein molecules diffuse close the surface, they may reorient and localized favorable electrostatic interactions may facilitate sorption to the hematite surface, as suggested in molecular dynamics (MD) simulations investigating the interactions of charged proteins with surfaces of identical charge [49, 50].

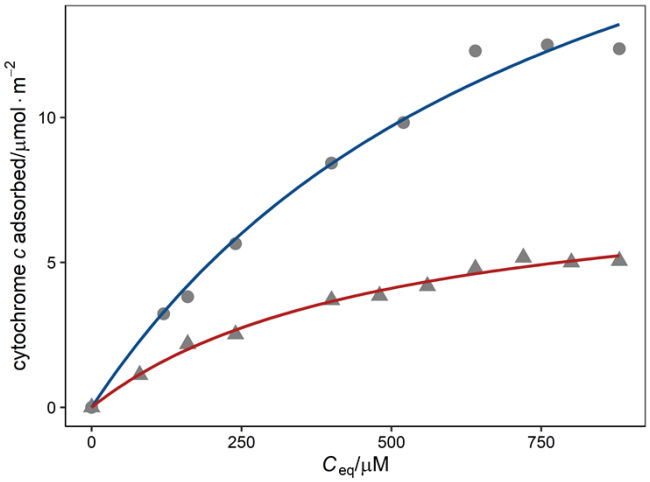

Figure 5. Adsorption isotherms of cyt *c* on hematite nanowire-array electrodes and fits to the Langmuir isotherm at 293 K for pH 4.3 (gray triangles, red line) and pH 7.07 (gray circles, blue lines). Langmuir fit parameters, pH 4.3: $Q_m = 8.17 \pm 0.54$ μmol·m^{-2}, $b = 2.02 \cdot 10^{-3} \pm 2.89 \cdot 10^{-4}$; pH 7.07: $Q_m = 23.38 \pm 3.11$ μmol·m^{-2}, $b = 1.47 \cdot 10^{-3} \pm 3.59 \cdot 10^{-4}$.

As the pH decreases from 7 to 4, the mineral surface becomes increasingly positively charged, leading to repulsive Coulombic forces between protein molecules and the surface. As a consequence, the cyt *c* sorption capacity decreases. The adsorbed amounts of native and partially unfolded cyt *c* in different pH buffers derived from isotherm fits are listed in Table 1 (Figure S7). In neutral pH buffer, the amount of native cyt *c* adsorbed was substantially higher than that of the partially unfolded form; however, in the acidic buffer of pH 4.3, more of the partially unfolded form than the native cyt *c* was adsorbed (Table 1). These data are consistent with the discussion above that decreasing pH induced a conformational change of cyt *c* upon sorption.

Table 1. The monolayer adsorption capacity of native, partially unfolded and total cyt *c* in different pH buffers. The values are derived from Langmuir isotherm fits, based on the estimated surface area for the textured surface of hematite nanowires.

Q_m (μmol·m^{-2}), **cyt *c***	**pH 7.07**	**pH 4.3**
Native form (μmol·m^{-2})	21.10 ± 4.30	3.69 ± 0.48
Partially unfolded form (μmol·m^{-2})	4.48 ± 0.58	4.51 ± 0.21
Protein total (μmol·m^{-2})	23.38 ± 3.11	8.17 ± 0.54

3.5 Electron transfer rate between cyt *c* and hematite

Dynamic electrochemical techniques are used extensively to measure and analyze electron transfer rates of redox-active species adsorbed to electrodes [51]. If the interfacial electron transfer is not limited by mass transport, the current response to applied potentials shows the direct electron transfer between the redox centers of adsorbed protein and the electrode. In the case of cyt *c* we have established above that it readily adsorbs on the surface of hematite with about 93% coverage at pH 7.07. Thus cyclic voltammetry is an appropriate means to determine the rate constant of direct electron transfer between cyt *c* and hematite minerals, where variations of peak positions as a function of the scan rate [33] are analyzed (Figure S8). The cathodic peak potential E_{pc} and anodic peak potential E_{pa} of the native (Figure 6a) and partially unfolded (Figure 6b) cyt *c* are plotted as a function of scan rate on a log scale. The CV measurements were carried out in 120 μM cyt *c* buffer solution (pH 7.07) with varying scan rates. At low scan rates (from 5 mV·s^{-1} to 250 mV·s^{-1}), the cathodic and anodic peak potentials exhibit a linear dependence on the scan rate, demonstrating a surface-controlled electrochemical behavior of the adsorbed cyt *c*. At higher scan rates (from 400 mV·s^{-1} to 1 V·s^{-1}), the separation between reductive and oxidative peaks is more pronounced, as shown in the so-called trumpet plot.

These current-potential response results are consistent with previous reports [51]: as the applied voltage is slowly increased (i.e., low scan rate), the system of an uncoupled one-electron redox reaction is maintained at equilibrium. Under these conditions the time required for electron transfer between the electrode and redox centers is being met. As the scan rate is increased, the time required for electron transfer remains the same, but the current response lags behind the applied potential, resulting in the maximal current observed at a greater separation of cathodic and anodic peaks. Fitting the scan rate dependence of the peak potential using a Butler-Volmer description of a single adsorbed redox center, based on the method described by Laviron [33], yields a first order rate constant for interfacial electron transfer of k^o_{ET} = 0.4 s^{-1} for the native form and k^o_{ET} = 0.55 s^{-1} for the partially unfolded form (Figure 6).

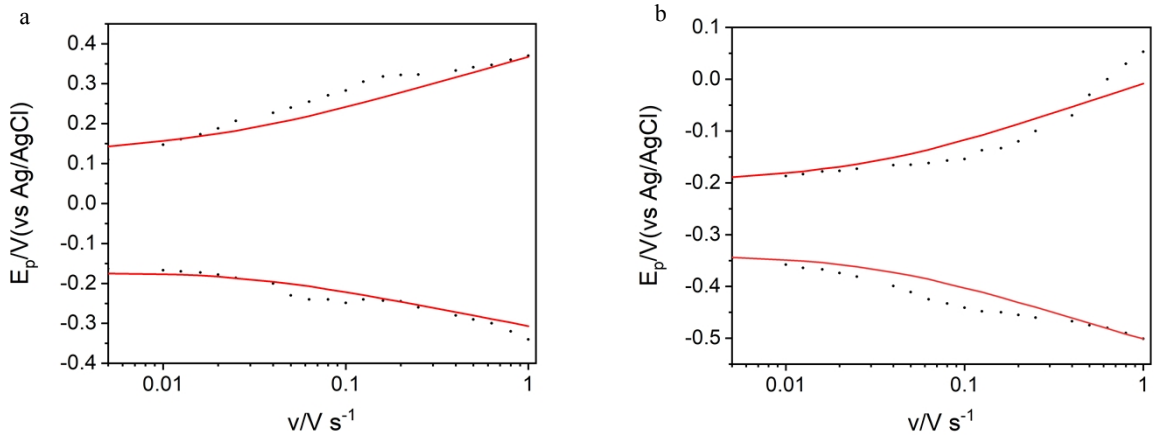

Figure 6. Scan rate dependence of cathodic and anodic peak potentials determined from CV measurements of cyt *c* at a hematite nanowire array electrode with Ag/AgCl (sat. KCl) as the reference electrode in Tris-HCl buffer (pH 7.07) with 120 μM cyt *c* (black dots). (a) native form (b) partially unfolded form. Fits to the Butler-Volmer equation (red lines) were obtained using Jellyfit (see text).

These values are smaller than those obtained for cyt *c* interacting with other electrode materials, such as gold nanoparticle electrode [19, 52, 53]. For example, the k^o_{ET} for cyt *c* on a gold electrode with a self-assembled monolayer of 11-mercaptoundecanoic acid was 13 s^{-1}, which is about 20-fold higher than the rate for the hematite electrode used in our study. This difference appears reasonable because hematite, as a semiconductor, is less conductive than a gold electrode, it therefore transfers electrons from cyt *c* less efficiently than gold.

To evaluate AQDS as a shuttle molecule facilitating electron transfer at the hematite surface, fast scan voltammetry was used to measure the current-potential response curve in the presence of 20 μM AQDS at near neutral pH. For the small redox molecule, diffusion-controlled treatment was used to analyze the relationship of peak potentials and scan rates [54](see their Eq. 26). With the transfer coefficient β of 0.35, the electron transfer rate was derived from data in Figure S9 as: $k^o_{ET} = 8.0 \cdot 10^{-3} \pm 0.2 \cdot 10^{-3}$ cm·s^{-1}. To compare this diffusion controlled electron transfer rate with the first order rate constant for interfacial electron transfer of adsorbed proteins, we use 10 μm as a distance of diffusion in a biofilm. The rate of electron transfer across this distance is calculated to be $8.0 \cdot 10^{-3}$ cm·s^{-1} / 10 μm = 8.0 s^{-1}, which is much greater than the rates (k^o_{ET} = 0.4 s^{-1} for the native form and k^o_{ET} = 0.55 s^{-1} for the partially unfolded) between hematite and cyt *c*.

In vivo experiments have demonstrated that addition of AQDS to DIRB cells stimulated Fe(III) reduction by removing the need for microbes to directly contact minerals [26, 27]. Compared with direct electron transfer between surface adsorbed protein redox centers, AQDS transfers electrons to hematite surface at a faster rate than cyt *c*, thus our data support the in vivo experimental results. While the electron transfer between hematite and AQDS in solution is diffusion-controlled, we do not know if electron transfer between AQDS and the redox centers of microbial proteins (i.e., outer membrane cytochromes) is rate limiting. This is beyond the current scope of the study and future research is needed.

4 Conclusion

We investigated the interaction of a hematite nanowire array electrode with horse heart cytochrome *c* as a model system for redox-active proteins. Cyclic voltammetry demonstrated direct electron transfer between the cyt *c* and the electrode surface. Two pairs of distinct redox peaks are consistent with the existence of two conformations of cyt *c* upon adsorption, the native form and a partially unfolded form. The mid-point potentials at pH 7.07 are -15 mV and -278 mV for the native and partially unfolded conformations, respectively. The solution pH has a substantial influence on the conformation of the protein, its sorption, and electron transfer: at near neutral pH, the majority of protein maintains its native state (84%), and readily adsorbs on the surface of hematite (total coverage of 93% of which 21.1 $\mu mol \cdot m^{-2}$ is in the native form). This direct contact between cyt *c* and hematite enables the exchange of electrons with the hematite mineral electrode. Shifting the pH to more acidic values (~pH 4), the majority of the protein assumes a partially unfolded conformation (55%). This partially unfolded form of cyt *c* maintained redox reactivity, although at a lower midpoint potential (-278 mV) compared to that of the native form (-35 mV) at pH 4.66. At alkaline pH, the mineral surface is chemically unstable and electron transfer rates cannot be determined by electrochemical methods.

The electron transfer rates of cyt *c* adsorbed to hematite were 0.4 s^{-1} (native form) and 0.55 s^{-1} (partially unfolded form), respectively. These rates were slower than electron transfer between hematite and the electron shuttling compound AQDS if the the diffusional distance is less than 100 μm, because the rate constant for AQDS is $8.0 \cdot 10^{-3}$ $cm \cdot s^{-1}$ at neutral pH. The modes of electron transfers are distinct: AQDS interacts with hematite through a diffusion-controlled mechanism, while cyt *c* strongly adsorbs to the surface of hematite. Although AQDS is capable of transferring electrons to hematite, rates of electron exchange between proteins and AQDS remain unknown requiring further research. This study contributes to our understanding of the complex interactions between metal oxides, redox-active biological macromolecules and ultimately cells, enabling insights into more complex chemical transformations at cell-mineral interfaces.

Acknowledgements

This research was sponsored by the Laboratory Directed Research and Development Program of Oak Ridge National Laboratory, managed by UT-Battelle, LLC, for the U.S. Department of Energy (Project ID 8174), under Contract No. DE-AC05-00OR22725 with the U.S. Department of Energy. The United States Government retains and the publisher, by accepting the article for publication, acknowledges that the United States Government retains a non-exclusive, paid-up, irrevocable, worldwide license to publish or reproduce the published form of this manuscript, or allow others to do so, for United States Government purposes. The Department of Energy will provide public access to these results of federally sponsored research in accordance with the DOE Public Access Plan (http://energy.gov/downloads/doe-public-access-plan).

Supplemental Information

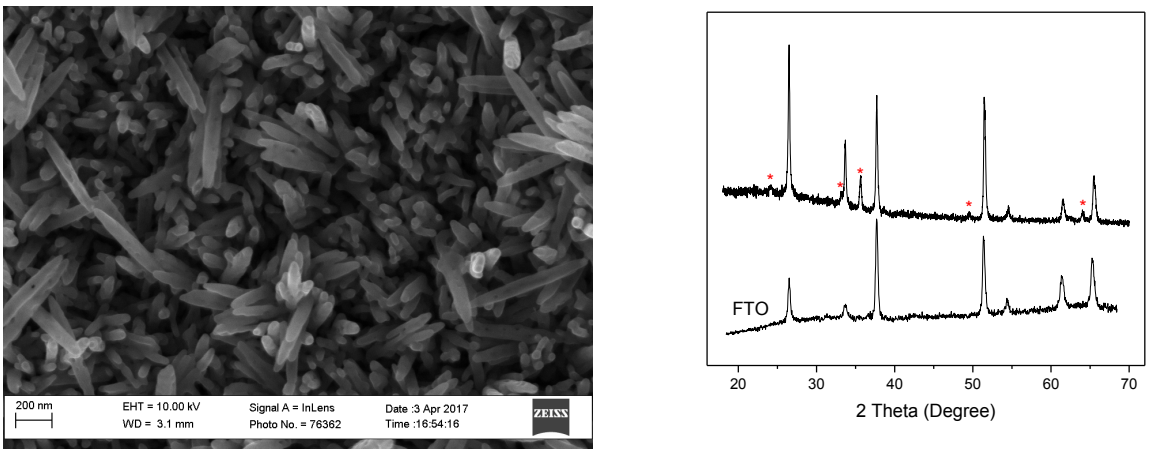

Figure S1. Left: SEM image of hematite nanowires on the FTO substrate. Scale bar is 200 nm. Right: XRD pattern collected from hematite nanowires on the FTO substrate (top). XRD pattern (bottom) of FTO substrate are provided as reference. The five diffraction peaks marked by asterisks are identified in the XRD pattern, which can be indexed as hematite, alpha-phase Fe_2O_3 (JCPDS, No. 33-0664). The absence of β-FeOOH diffraction peaks indicates the complete conversion of β-FeOOH to α-Fe_2O_3.

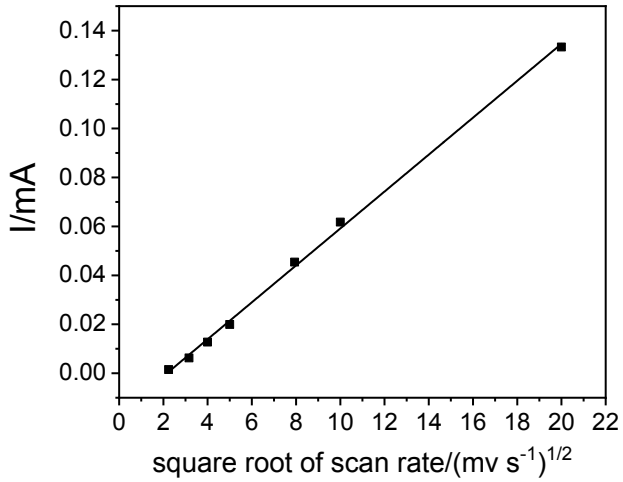

Figure S2. Current vs. square root of scan rate for AQDS (20 μM) with a hematite nanowire array working electrode in Tris-HCl buffer (pH 7.07) demonstrating the diffusion-controlled behavior. The Ag/AgCl (sat. KCl) was used as the reference electrode.

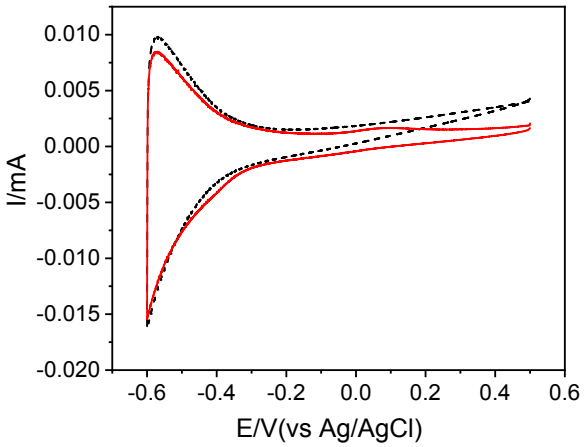

Figure S3. Cyclic voltammogram data collected from a hematite nanowire electrode, using a background solution of Tris-HCl medium at pH 9.84 (black dashed line) and 40 μM cyt *c* in Tris-HCl buffer (red solid line). The scan rate is 10 $mV \cdot s^{-1}$ with Ag/AgCl (sat. KCl) as the reference electrode.

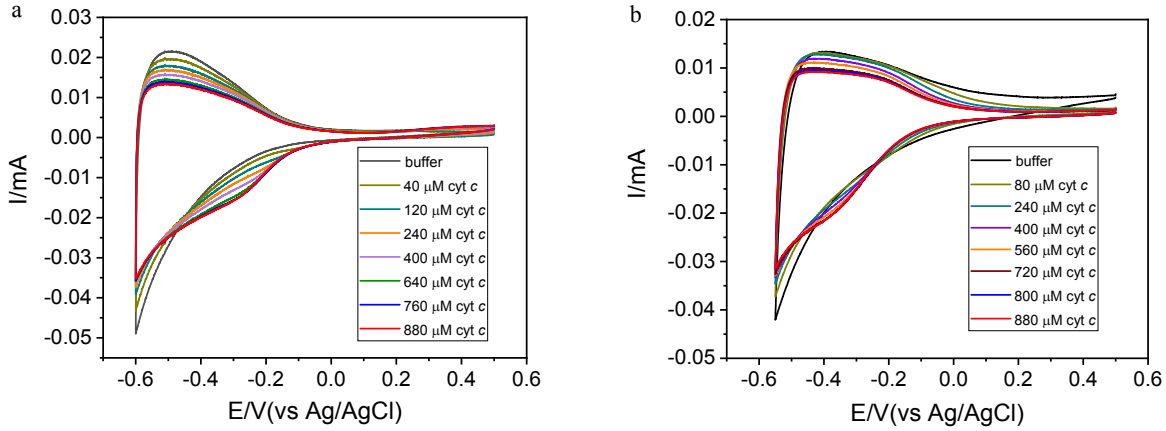

Figure S4. Cyclic voltammetry data collected from a hematite nanowire array electrode in Tris-HCl buffer at different concentrations of cyt *c* and at (a) pH 7.07 and (b) pH 4.3. The scan rate is 10 $mV \cdot s^{-1}$ with Ag/AgCl (sat. KCl) as the reference electrode. Examples of reduction curves with selected concentrations are given in Figure S5 for pH 7.07, and in Figure S6 for pH 4.3.

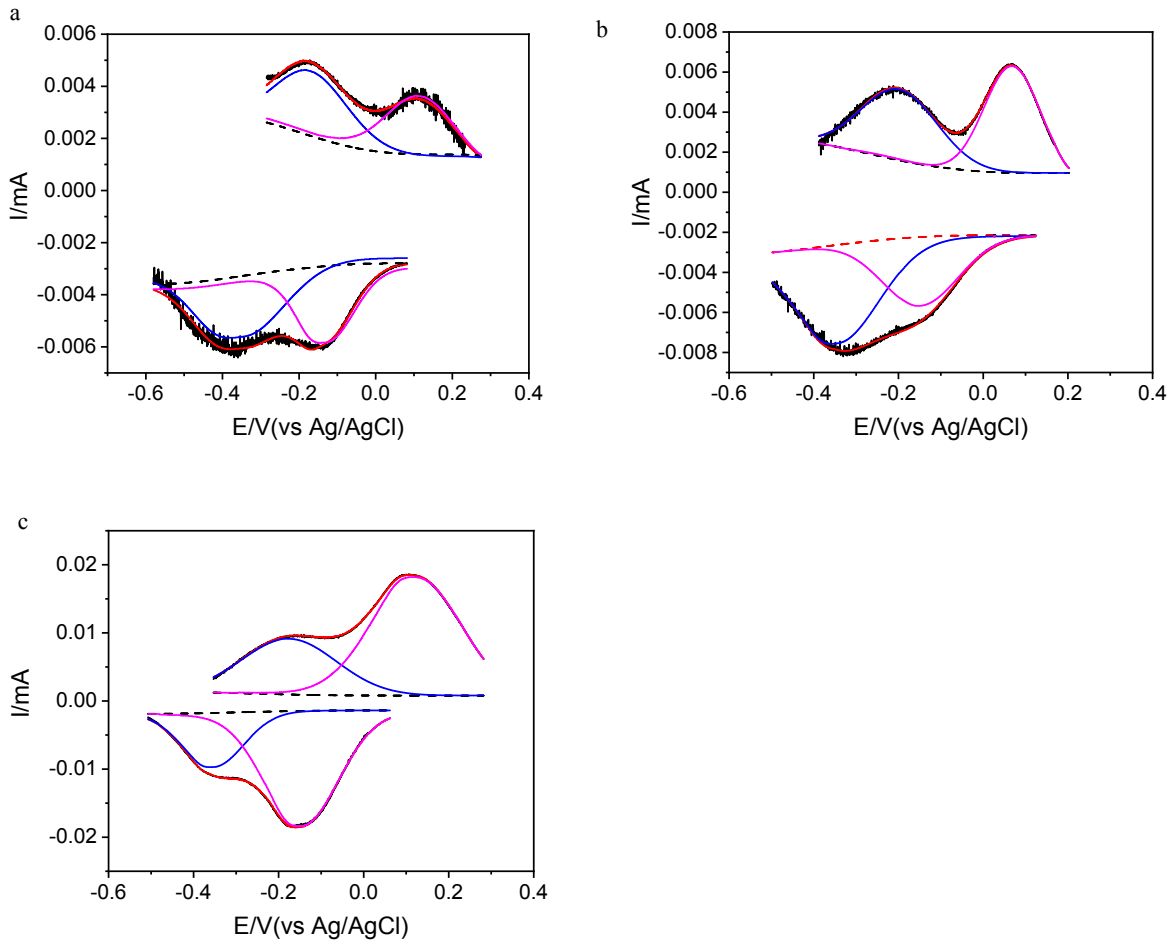

Figure S5. The reduction curves with different concentrations of cyt *c* (a: 80 μM; b: 120 μM; c: 880 μM) from the CV data in (Figure S4 a, pH 7.07) after background subtraction and peak deconvolution. Each line represents: raw data (black), background (dashed black), peak sum (red), native form of cyt *c* (magenta) and partially unfolded form of cyt *c* (blue).

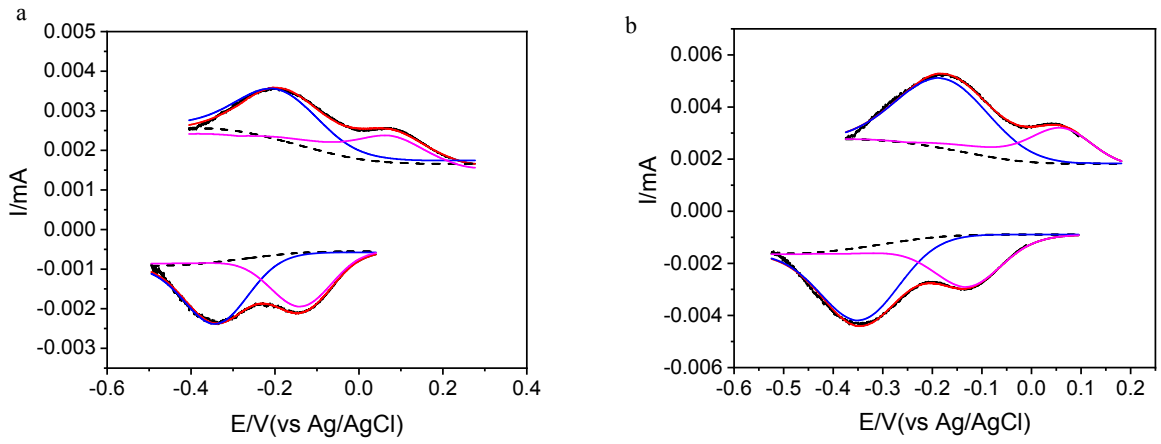

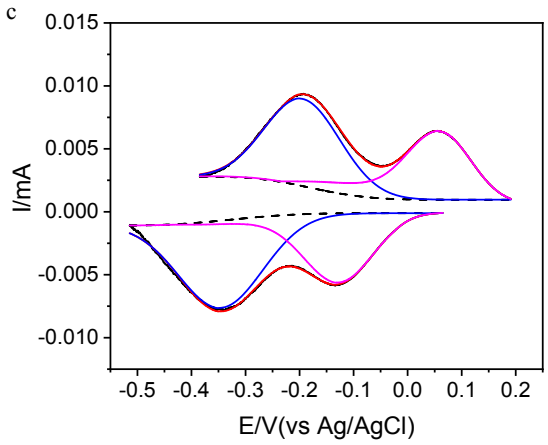

Figure S6. The reduction curves with different concentrations of cyt *c* (a: 80 μM; b: 160 μM; c: 880 μM) from the CV data in (Figure S4 b, pH 4.3) after background subtraction and peak deconvolution. Each line represents: raw data (black), background (dashed black), peak sum (red), native form of cyt *c* (magenta) and partially unfolded form of cyt *c* (blue).

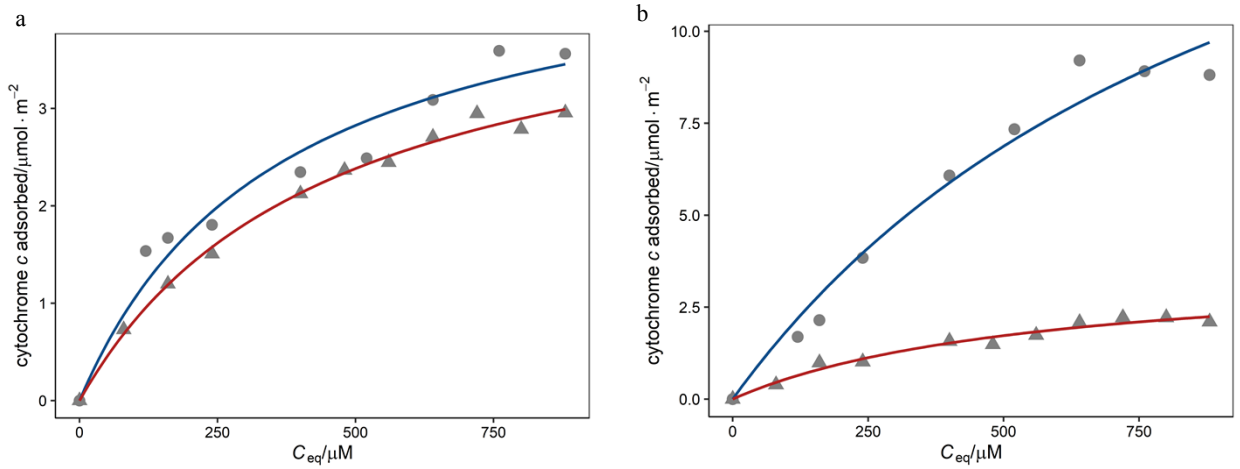

Figure S7. Adsorption isotherms of cyt *c* (a: partially unfolded form; b: native form) on a hematite nanowire array electrode as a function of cyt *c* equilibrium concentrations (C_{eq}). Solid lines represent fits to the Langmuir isotherm at 293 K derived from charge transferred for each at pH 4.3 (red) and pH 7.07 (blue). Langmuir fit parameters of partially unfolded form of cyt *c*: pH 4.3: $Q_m = 4.51 \pm 0.21$ μmol·m^{-2}, $b = 2.24 \cdot 10^{-3} \pm 2.37 \cdot 10^{-4}$; pH 7.0: $Q_m = 4.58 \pm 0.58$ μmol·m^{-2}, $b = 2.75 \cdot 10^{-3} \pm 7.82 \cdot 10^{-4}$.

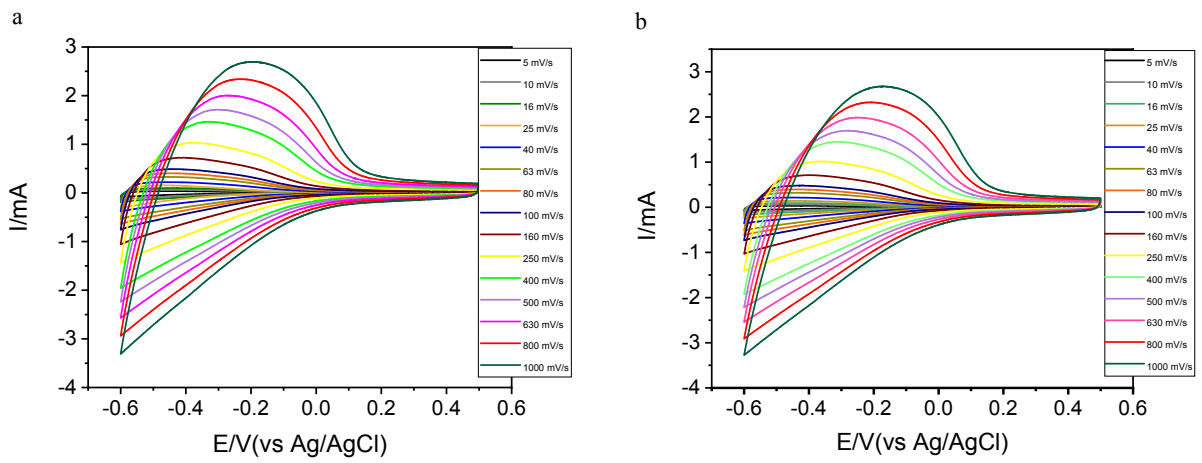

Figure S8. Cyclic voltammetry data collected from a hematite nanowire-array electrode, using a (a) background of Tris-HCl medium at pH 7.07 and (b) 120 μM cyt *c* in the same Tris-HCl at various scan rates. The Ag/AgCl (sat. KCl) was used as the reference electrode.

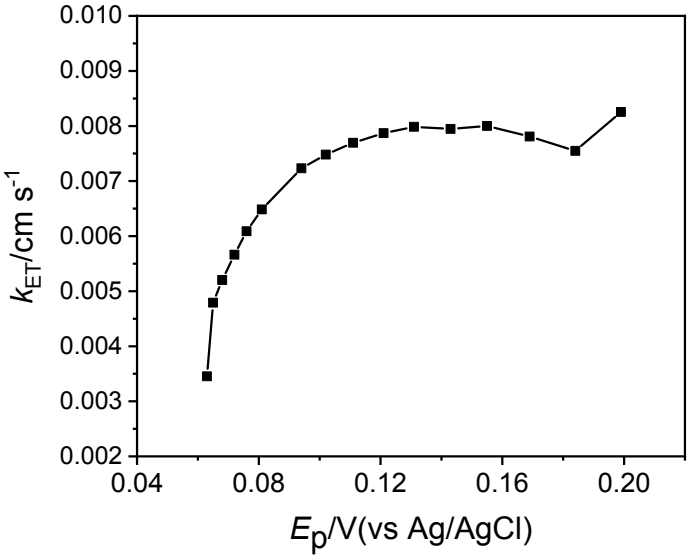

Figure S9. Variation of the CV peak separation (E_p=E_{pa}-E_{pc}) with the value of k_{ET} evaluated from the approach by Klingler and Kochi [54] for 20 μM AQDS in Tris-HCl buffer (pH 7.07). The values of k_{ET} for AQDS become independent of the peak separation and scan rate beyond ~150 mV, and this limiting value is reported as of $k^o_{ET} = 8.0 \cdot 10^{-3} \pm 0.2 \cdot 10^{-3}$ cm·s^{-1}.

References

[1] D.R. Lovley, Bug juice: harvesting electricity with microorganisms, Nature Reviews Microbiology, 4 (2006) 497. https://doi.org/10.1038/nrmicro1442

[2] H. Wang, F. Qian, Y. Li, Solar-assisted microbial fuel cells for bioelectricity and chemical fuel generation, Nano Energy, 8 (2014) 264-273. https://doi.org/10.1016/j.nanoen.2014.06.004

[3] H. Wang, F. Qian, G. Wang, Y. Jiao, Z. He, Y. Li, Self-Biased Solar-Microbial Device for Sustainable Hydrogen Generation, ACS Nano, 7 (2013) 8728-8735. https://doi.org/10.1021/nn403082m

[4] F. Qian, H. Wang, Y. Ling, G. Wang, M.P. Thelen, Y. Li, Photoenhanced Electrochemical Interaction between Shewanella and a Hematite Nanowire Photoanode, Nano Letters, 14 (2014) 3688-3693. https://doi.org/10.1021/nl501664n

[5] B.M. Fonseca, C.M. Paquete, C.A. Salgueiro, R.O. Louro, The role of intramolecular interactions in the functional control of multiheme cytochromes c, FEBS Letters, 586 (2012) 504-509. https://doi.org/10.1016/j.febslet.2011.08.019

[6] M.J. Edwards, A.J. Gates, J.N. Butt, D.J. Richardson, T.A. Clarke, Comparative structure-potentio-spectroscopy of the Shewanella outer membrane multiheme cytochromes, Current Opinion in Electrochemistry, 4 (2017) 199-205. https://doi.org/10.1016/j.coelec.2017.08.013

[7] David J. Richardson, Marcus J. Edwards, Gaye F. White, N. Baiden, Robert S. Hartshorne, J. Fredrickson, L. Shi, J. Zachara, Andrew J. Gates, Julea N. Butt, Thomas A. Clarke, Exploring the biochemistry at the extracellular redox frontier of bacterial mineral Fe(III) respiration, Biochemical Society Transactions, 40 (2012) 493. https://doi.org/10.1042/BST20120018

[8] L. Shi, J. Richardson David, Z. Wang, N. Kerisit Sebastien, M. Rosso Kevin, M. Zachara John, K. Fredrickson James, The roles of outer membrane cytochromes of Shewanella and Geobacter in extracellular electron transfer, Environmental Microbiology Reports, 1 (2009) 220-227. https://doi.org/10.1111/j.1758-2229.2009.00035.x

[9] L. Shi, H. Dong, G. Reguera, H. Beyenal, A. Lu, J. Liu, H.-Q. Yu, J.K. Fredrickson, Extracellular electron transfer mechanisms between microorganisms and minerals, Nature Reviews Microbiology, 14 (2016) 651. https://doi.org/10.1038/nrmicro.2016.93

[10] C.M. Eggleston, J. Vörös, L. Shi, B.H. Lower, T.C. Droubay, P.J.S. Colberg, Binding and direct electrochemistry of OmcA, an outer-membrane cytochrome from an iron reducing bacterium, with oxide electrodes: A candidate biofuel cell system, Inorganica Chimica Acta, 361 (2008) 769-777. https://doi.org/10.1016/j.ica.2007.07.015

[11] A. Johs, L. Shi, T. Droubay, J.F. Ankner, L. Liang, Characterization of the Decaheme c-Type Cytochrome OmcA in Solution and on Hematite Surfaces by Small Angle X-Ray Scattering and Neutron Reflectometry, Biophysical Journal, 98 (2010) 3035-3043. https://doi.org/10.1016/j.bpj.2010.03.049

[12] A. El Kasmi, M.C. Leopold, R. Galligan, R.T. Robertson, S.S. Saavedra, K. El Kacemi, E.F. Bowden, Adsorptive immobilization of cytochrome c on indium/tin oxide (ITO): electrochemical evidence for electron transfer-induced conformational changes, Electrochemistry Communications, 4 (2002) 177-181. https://doi.org/10.1016/S1388-2481(01)00299-5

[13] A. Kowalsky, A Study of the Mechanism of Electron Transfer in Cytochrome c, The Journal of Biological Chemistry, 244 (1969) 6619-6625.

[14] M.O. Hengartner, The biochemistry of apoptosis, Nature, 407 (2000) 770. https://doi.org/10.1038/35037710

[15] C.M. Eggleston, N. Khare, D.M. Lovelace, Cytochrome c interaction with hematite (α-Fe2O3) surfaces, Journal of Electron Spectroscopy and Related Phenomena, 150 (2006) 220-227. https://doi.org/10.1016/j.elspec.2005.06.006

[16] N. Khare, C.M. Eggleston, D.M. Lovelace, Sorption and direct electrochemistry of mitochondrial cytochrome C on hematite surfaces, Clays and Clay Minerals, 53 (2005) 564-571. https://doi.org/10.1346/CCMN.2005.0530602
[17] E.F. Bowden, F.M. Hawkridge, H.N. Blount, Interfacial electrochemistry of cytochrome c at tin oxide, indium oxide, gold, and platinum electrodes, Journal of Electroanalytical Chemistry and Interfacial Electrochemistry, 161 (1984) 355-376. https://doi.org/10.1016/S0022-0728(84)80193-X
[18] M.J. Tarlov, E.F. Bowden, Electron-transfer reaction of cytochrome c adsorbed on carboxylic acid terminated alkanethiol monolayer electrodes, Journal of the American Chemical Society, 113 (1991) 1847-1849. https://doi.org/10.1021/ja00005a068
[19] K. Murata, K. Kajiya, M. Nukaga, Y. Suga, T. Watanabe, N. Nakamura, H. Ohno, A Simple Fabrication Method for Three-Dimensional Gold Nanoparticle Electrodes and Their Application to the Study of the Direct Electrochemistry of Cytochrome c, Electroanalysis, 22 (2010) 185-190. https://doi.org/10.1002/elan.200900323
[20] N. Khare, D.M. Lovelace, C.M. Eggleston, M. Swenson, T.S. Magnuson, Redox-linked conformation change and electron transfer between monoheme c-type cytochromes and oxides, Geochimica et Cosmochimica Acta, 70 (2006) 4332-4342. https://doi.org/10.1016/j.gca.2006.06.1561
[21] Y. Tokunou, K. Hashimoto, A. Okamoto, Acceleration of Extracellular Electron Transfer by Alternative Redox-Active Molecules to Riboflavin for Outer-Membrane Cytochrome c of Shewanella oneidensis MR-1, The Journal of Physical Chemistry C, 120 (2016) 16168-16173. https://doi.org/10.1021/acs.jpcc.6b00349
[22] N.J. Kotloski, J.A. Gralnick, Flavin Electron Shuttles Dominate Extracellular Electron Transfer by Shewanella oneidensis, mBio, 4 (2013) e00553-00512. https://doi.org/10.1128/mBio.00553-12
[23] A. Okamoto, K. Hashimoto, K.H. Nealson, R. Nakamura, Rate enhancement of bacterial extracellular electron transport involves bound flavin semiquinones, Proceedings of the National Academy of Sciences, 110 (2013) 7856. https://doi.org/10.1073/pnas.1220823110
[24] A. Okamoto, S. Kalathil, X. Deng, K. Hashimoto, R. Nakamura, K.H. Nealson, Cell-secreted Flavins Bound to Membrane Cytochromes Dictate Electron Transfer Reactions to Surfaces with Diverse Charge and pH, Scientific Reports, 4 (2014) 5628. https://doi.org/10.1038/srep05628
[25] C. Liu, J.M. Zachara, N.S. Foster, J. Strickland, Kinetics of Reductive Dissolution of Hematite by Bioreduced Anthraquinone-2,6-disulfonate, Environmental Science & Technology, 41 (2007) 7730-7735. https://doi.org/10.1021/es070768k
[26] M.P. Manzella, G. Reguera, K. Kashefi, Extracellular Electron Transfer to Fe(III) Oxides by the Hyperthermophilic Archaeon Geoglobus ahangari via a Direct Contact Mechanism, Appl. Environ. Microbiol., 79 (2013) 4694-4700. https://doi.org/10.1128/AEM.01566-13
[27] D. Liu, H. Dong, L. Zhao, H. Wang, Smectite Reduction by Shewanella Species as Facilitated by Cystine and Cysteine, Geomicrobiology Journal, 31 (2014) 53-63. https://doi.org/10.1080/01490451.2013.806609
[28] S. Kato, K. Hashimoto, K. Watanabe, Microbial interspecies electron transfer via electric currents through conductive minerals, Proceedings of the National Academy of Sciences, 109 (2012) 10042. https://doi.org/10.1073/pnas.1117592109
[29] M.F. Hochella, S.K. Lower, P.A. Maurice, R.L. Penn, N. Sahai, D.L. Sparks, B.S. Twining, Nanominerals, Mineral Nanoparticles, and Earth Systems, Science, 319 (2008) 1631. https://doi.org/10.1126/science.1141134
[30] D.R. Lovley, Dissimilatory Fe(III) and Mn(IV) Reduction, Microbiology and Molecular Biology Reviews, 55 (1991) 259-287 https://doi.org/0146-0749/91/020259-29$02.00/0
[31] E.D. Melton, E.D. Swanner, S. Behrens, C. Schmidt, A. Kappler, The interplay of microbially mediated and abiotic reactions in the biogeochemical Fe cycle, Nature Reviews Microbiology, 12 (2014) 797. https://doi.org/10.1038/nrmicro3347

[32] L.J.C. Jeuken, J.P. McEvoy, F.A. Armstrong, Insights into Gated Electron-Transfer Kinetics at the Electrode−Protein Interface: A Square Wave Voltammetry Study of the Blue Copper Protein Azurin, The Journal of Physical Chemistry B, 106 (2002) 2304-2313. https://doi.org/10.1021/jp0134291
[33] E. Laviron, General expression of the linear potential sweep voltammogram in the case of diffusionless electrochemical systems, Journal of Electroanalytical Chemistry and Interfacial Electrochemistry, 101 (1979) 19-28. https://doi.org/10.1016/S0022-0728(79)80075-3
[34] C. Feng, L. Ma, F. Li, H. Mai, X. Lang, S. Fan, A polypyrrole/anthraquinone-2,6-disulphonic disodium salt (PPy/AQDS)-modified anode to improve performance of microbial fuel cells, Biosens Bioelectron, 25 (2010) 1516-1520. https://doi.org/10.1016/j.bios.2009.10.009
[35] F. Cao, T.X. Liu, C.Y. Wu, F.B. Li, X.M. Li, H.Y. Yu, H. Tong, M.J. Chen, Enhanced Biotransformation of DDTs by an Iron- and Humic-Reducing Bacteria Aeromonas hydrophila HS01 upon Addition of Goethite and Anthraquinone-2,6-Disulphonic Disodium Salt (AQDS), Journal of Agricultural and Food Chemistry, 60 (2012) 11238-11244. https://doi.org/10.1021/jf303610w
[36] S. Orsetti, C. Laskov, S.B. Haderlein, Electron Transfer between Iron Minerals and Quinones: Estimating the Reduction Potential of the Fe(II)-Goethite Surface from AQDS Speciation, Environmental Science & Technology, 47 (2013) 14161-14168. https://doi.org/10.1021/es403658g
[37] C. Batchelor-McAuley, Q. Li, S.M. Dapin, R.G. Compton, Voltammetric Characterization of DNA Intercalators across the Full pH Range: Anthraquinone-2,6-disulfonate and Anthraquinone-2-sulfonate, The Journal of Physical Chemistry B, 114 (2010) 4094-4100. https://doi.org/10.1021/jp1008187
[38] X. Chen, R. Ferrigno, J. Yang, G.M. Whitesides, Redox Properties of Cytochrome c Adsorbed on Self-Assembled Monolayers: A Probe for Protein Conformation and Orientation, Langmuir, 18 (2002) 7009-7015. https://doi.org/10.1021/la0204794
[39] D.L. Pilloud, X. Chen, P.L. Dutton, C.C. Moser, Electrochemistry of Self-Assembled Monolayers of Iron Protoporphyrin IX Attached to Modified Gold Electrodes through Thioether Linkage, The Journal of Physical Chemistry B, 104 (2000) 2868-2877. https://doi.org/10.1021/jp992776w
[40] P. Hildebrandt, M. Stockburger, Cytochrome c at charged interfaces. 1. Conformational and redox equilibria at the electrode/electrolyte interface probed by surface-enhanced resonance Raman spectroscopy, Biochemistry, 28 (1989) 6710-6721. https://doi.org/10.1021/bi00442a026
[41] J. Haladjian, R. Pilard, P. Bianco, P.-A. Serre, Effect of pH on the electroactivity of horse heart cytochrome c, Bioelectrochemistry and Bioenergetics, 9 (1982) 91-101. https://doi.org/10.1016/0302-4598(82)80008-1
[42] L. Konermann, D.J. Douglas, Acid-Induced Unfolding of Cytochrome c at Different Methanol Concentrations: Electrospray Ionization Mass Spectrometry Specifically Monitors Changes in the Tertiary Structure, Biochemistry, 36 (1997) 12296-12302. https://doi.org/10.1021/bi971266u
[43] M. Fedurco, J. Augustynski, C. Indiani, G. Smulevich, M. Antalík, M. Bánó, E. Sedlák, M.C. Glascock, J.H. Dawson, Electrochemistry of Unfolded Cytochrome c in Neutral and Acidic Urea Solutions, Journal of the American Chemical Society, 127 (2005) 7638-7646. https://doi.org/10.1021/ja050321g
[44] L. Wang, D.H. Waldeck, Denaturation of Cytochrome c and Its Peroxidase Activity When Immobilized on SAM Films, The Journal of Physical Chemistry C, 112 (2008) 1351-1356. https://doi.org/10.1021/jp076807w
[45] K. Shimizu, A. Lasia, J.-F. Boily, Electrochemical Impedance Study of the Hematite/Water Interface, Langmuir, 28 (2012) 7914-7920. https://doi.org/10.1021/la300829c
[46] K. Bindu, S. Kishore, K.M. Ajith, H.N. Lim, H.S. Nagaraja, Microwave assisted growth of stannous ferrite microcubes as electrodes for potentiometric nonenzymatic H2O2 sensor and supercapacitor applications, Electrochimica Acta, 217 (2016) 139-149. https://doi.org/10.1016/j.electacta.2016.09.083
[47] S. Magdassi, Surface activity of proteins: Chemical and physicochemical modifications, 1st ed., CRC Press1996.

[48] L. Liang, J.J. Morgan, Chemical aspects of iron oxide coagulation in water: Laboratory studies and implications for natural systems, Aquatic Sciences, 52 (1990) 32-55. https://doi.org/10.1007/BF00878240
[49] K. Kubiak-Ossowska, B. Jachimska, P.A. Mulheran, How Negatively Charged Proteins Adsorb to Negatively Charged Surfaces: A Molecular Dynamics Study of BSA Adsorption on Silica, The Journal of Physical Chemistry B, 120 (2016) 10463-10468. https://doi.org/10.1021/acs.jpcb.6b07646
[50] C. Peng, J. Liu, Y. Xie, J. Zhou, Molecular simulations of cytochrome c adsorption on positively charged surfaces: the influence of anion type and concentration, Physical Chemistry Chemical Physics, 18 (2016) 9979-9989. https://doi.org/10.1039/C6CP00170J
[51] C. Léger, P. Bertrand, Direct Electrochemistry of Redox Enzymes as a Tool for Mechanistic Studies, Chemical Reviews, 108 (2008) 2379-2438. https://doi.org/10.1021/cr0680742
[52] P.S. Jensen, Q. Chi, F.B. Grumsen, J.M. Abad, A. Horsewell, D.J. Schiffrin, J. Ulstrup, Gold Nanoparticle Assisted Assembly of a Heme Protein for Enhancement of Long-Range Interfacial Electron Transfer, The Journal of Physical Chemistry C, 111 (2007) 6124-6132. https://doi.org/10.1021/jp068453z
[53] A.F. Loftus, K.P. Reighard, S.A. Kapourales, M.C. Leopold, Monolayer-Protected Nanoparticle Film Assemblies as Platforms for Controlling Interfacial and Adsorption Properties in Protein Monolayer Electrochemistry, Journal of the American Chemical Society, 130 (2008) 1649-1661. https://doi.org/10.1021/ja076312k
[54] R.J. Klingler, J.K. Kochi, Electron-transfer kinetics from cyclic voltammetry. Quantitative description of electrochemical reversibility, The Journal of Physical Chemistry, 85 (1981) 1731-1741. https://doi.org/10.1021/j150612a028